Investigation of Earthquake Deformation Detectability Using Sentinel-1 Interferometric Data

Djenaliev, A.,[1*] Kada, M.,[1] Chymyrov, A.,[2] Hellwich, O.[1] Bairamov, E.,[1,3] and Muraliev, A.[4]
[1]Technical University of Berlin, Berlin, Germany
E-mail: djakjol@mailbox.tu-berlin.de, martin.kada@tu-berlin.de, olaf.hellwich@tu-berlin.de
[2]I.Razzakov Kyrgyz State Technical University, Bishkek, Kyrgyzstan
E-mail: akylbek.chymyrov@aca-giscience.org
[3]Nazarbayev University, Astana, Kazakhstan, E-mail: emil.bayramov@nu.edu.kz
[4]Institute of Seismology, National Academy of Science, Bishkek, Kyrgyzstan, E-mail: abmuraliev@mail.ru
**Corresponding Author*

DOI: https://doi.org/10.52939/ijg.v18i6.2453

Abstract
Historically, the Kyrgyz Republic and neighboring countries have experienced numerous strong earthquakes. Our research focused on the investigation of surface deformations caused by 5 earthquake events which had occurred during 2014-2017. A Differential Interferometric Synthetic Aperture Radar (DInSAR) technique was applied for the Sentinel-1 Interferometric data acquired before and after earthquake events. The pairs of images were processed using the SNAP software to produce a coseismic interferogram, coherence and displacement maps.

Keywords: Deformation, Displacement, Earthquake, Interferogram, Coherence, Radar

1. Introduction

Earthquake can be described as a result of the sudden slip on a fault and ground shaking caused by release of energy stored in the Earth crust, which creates seismic wave at its source [1]. This event is considered as the deadliest and the most catastrophic natural disaster. The strong earthquakes are manifested by various deformations on the Earth surface, which are accompanied with secondary hazards such as landslides, rockfalls, and floods covering large areas. The destruction of buildings and man-made structures during an earthquake contribute to panic growth among population and increase human casualties [2].

The size of earthquakes usually measured in two ways, based on Magnitude (M) and Intensity (I). Magnitude term first introduced by Richter in 1935 [3]. The Richter scale provides a concept of the volume of energy released during an earthquake and the amplitude produced on a seismograph [1]. The influence of ground shaking on buildings and engineering structures over the earthquake affected region is measured through macroseismic intensity scale [4]. The well-known intensity scales are the Modified Mercalli scale (MM) [5], the Medvedev–Sponheuer–Karnik (MSK-64) [6], the European Macroseismic Scaleas (EMS-98) [7], which are used in different countries. The use of intensity scale is necessary for classification of the damage grade to different types of buildings and structures [4]. The observed intensity data is categorized with contour lines classifying regions of ground shaking intensity on a map, which is known as isoseismic or intensity maps. These maps provide valuable information regarding a spatial extent and a distribution of shaking intensity, and the response of buildings and population exposure to earthquakes. The use of macroseismic intensity scale is very important for vulnerability and seismic risk assessment studies [2].

Earthquake studies are needed to detect a ground deformation caused by an earthquake that obviously creates risks for building damage. The traditional geodetic approach for ground deformation monitoring are based on the geodetic measurements using the Global Positioning System (GPS), which are precise but quite costly field survey works [8] with intensive and regular measurements in the earthquake affected areas. Therefore, remote sensing data can provide a support for rapid acquisition of pre- and post-earthquake information required for the Earth surface monitoring analysis [9].

The data acquired by remote sensing sensors are valuable source of information and important to interpret the nature of earthquake consequences. In particular, radar remote sensing data is very useful for researchers to detect an earthquake deformation analysis [10].

2. SAR for Earthquake Study

In the beginning of 1980, the first results of radar images on mapping the Earth surface and its topographical characteristics were published, which were very important for surface displacement analysis [11]. The application of SAR data helps researchers to measure changes of the Earth surface and to detect ground deformations. The Interferometric Synthetic Aperture Radar (InSAR) is a useful method, which has been widely used in natural hazard monitoring, topographic mapping, environmental and geosciences related research over the last three decades [12].

The radar microwave energy propagates through cloud coverage without signal loss by providing data under all weather conditions at any time of day and nighttime [13]. The electromagnetic waves, transmitted from the radar and backscattered from ground surface to the radar contribute to the generation of a digital image. Each pixel of SAR image contains a complex record of amplitude and phase information [14]. Amplitude is a reflectivity of backscattered radar signal [13]. The phase of the radar signal is the fraction of a wavelength, which is determined by the distance between the radar antenna and the illuminated target on the ground [12].

InSAR method is based on the phase information recorded by radar antenna to measure the distance from radar to the ground target. This method uses phase differences between two or more SAR observations of the same target area acquired from two different periods or slightly different positions [14] [15]. Differential Interferometry (DInSAR) is a unique technique for detecting and mapping of ground deformations and surface displacements produced by earthquakes [11]. This measurement is very precise with an accuracy of several millimeters to centimeters [16]. This accuracy is quite sufficient for detecting a coseismic deformations induced by a moderate earthquake with magnitude of Mw>5.0 depending on the depth of the epicenter [13].

Since the launch of the European Remote Sensing Satellite ERS-1 in 1991 by the European Space Agency (ESA) Programme, the application of InSAR techniques for earthquake studies attracted many researchers. After the first successful detection of the 1992 Landers earthquake with magnitude Mw=5.1 using the ERS-1 satellite data [17], the number of the scientific studies on detecting and investigating earthquakes significantly increased.

The earthquake study in [18] using ALOS/PALSAR (L-band) and ENVISAT/ASAR (C-band) satellite images was performed for Kyrgyzstan case. The Nura earthquake with a magnitude Mw=6.6 occurred on October 5, 2008 in the southeastern part of the country. By the combination of the ascending ALOS data and the descending ENVISAT data the coseismic displacement measurements were acquired, where the detected surface rupture has a horizontal length up-to 7 km and the vertical offset of about 80 cm. This earthquake caused 74 deaths and the complete destruction of buildings and infrastructures in the Nura village and induced a surface rupture along the tectonic fault [19]. With the development of the Sentinel-1 SAR satellite, the application of InSAR for natural hazard monitoring and earthquake studies has opened new perspectives. The Sentinel-1 data has been successfully applied for many studies [8] [10] [20] [21].

3. The Sentinel-1 mission

The Sentinel-1 mission is a part of the European Copernicus Programme conducted by the European Space Agency (ESA). Currently, this mission comprises of a constellation of two SAR satellites. The first Sentinel-1A satellite was successfully launched on April 3, 2014, and the second Sentinel-1B satellite was launched on April 25, 2016. These two satellites share the same orbital plane and each of them carries a C-band Synthetic Aperture Radar (SAR) instrument, capable of providing data in all weather conditions during the day and night time [22]. The repeat cycle has been reduced from 35 days for ERS-1 and ERS-2 to 12 days for Sentinel-1A and can still be reduced to 6 days in combination with Sentinel-1B satellites [23].

The Sentinel-1 satellites provide images with different ground resolution of down to 5 m and large spatial coverage of up-to 400 km in four acquisition modes: Stripmap, Interferometric Wide Swath, Extra Wide Swath and Wave modes. The Interferometric Wide Swath (IW) Mode of Sentinel-1 satellites is the main data acquisition mode that provides complete global coverage of all land surface, sea ice and coastal areas [22]. The application of IW mode will be of primary use in this research paper. The Sentinel-1 IW mode has three sub-swaths (IW1, IW2 and IW3) data sets that cover a large swath of 250 km at ground resolutions of 5 m in the range versus 20 m in azimuth.

Each sub-swath data contains a series of bursts, where each burst has been processed as a discrete Single Look Complex (SLC) data product [23].

4. Methodology

4.1 Earthquake and Sentinel-1 data Selection

The selection of an earthquake event based on magnitude and depth criteria. The global earthquake catalog from the United States Geological Survey (USGS) (https://earthquake.usgs.gov) and the earthquake catalog from the Institute of Seismology, National Academy of Science of the Kyrgyz Republic (https://seismo.kg) have been used. The selection criteria are focused on the strong earthquakes with magnitude of Mw > 5.0 and depth h < 20km, where the epicenters are located within the territory of the country and at neighboring countries near boundary of Kyrgyzstan that occurred between the years 2014-2021. This corresponds to the first year of the Sentinel-1 global data acquisition. In total 5 earthquake events were selected, where 3 earthquake epicenters were located within the territory of Kyrgyzstan and other 2 earthquakes were located in the neighboring China and Tajikistan.

For each selected earthquake event, the satellite images acquired before and after earthquake have been used. The selection of the Sentinle-1 Interferometric Wide-Swath (IW) data was based on the following criteria, a) sufficient coverage area for an earthquake induced deformation analysis; b) the earliest post-earthquake image acquisition date; c) the shortest temporal baseline between the pair images. It is necessary to mention, that perpendicular baseline describing geometric parameters between two satellites were not considered in the data selection process. Combination of images from ascending and descending or from the different satellite tracks and acquisition modes are not suitable for interferometry analysis. The search query for the Sentinle-1 IW data was performed to identify all available satellite tracks, considering both ascending and descending passes by using the Copernicus Open Access Hub (https://scihub.copernicus.eu). The Sentinel-1 IW pairs of images, acquired before and after earthquake event, and each image supporting dual polarization VH (Vertical transmit and Horizontal receive) and VV (Vertical transmit and Vertical receive) types were downloaded. The spatial distribution of the selected earthquakes and the corresponding sub-swath of the Sentine-1 IW images are presented in Figure 1. The details of earthquake parameter and Sentinle-1 IW data are shown in Table 1.

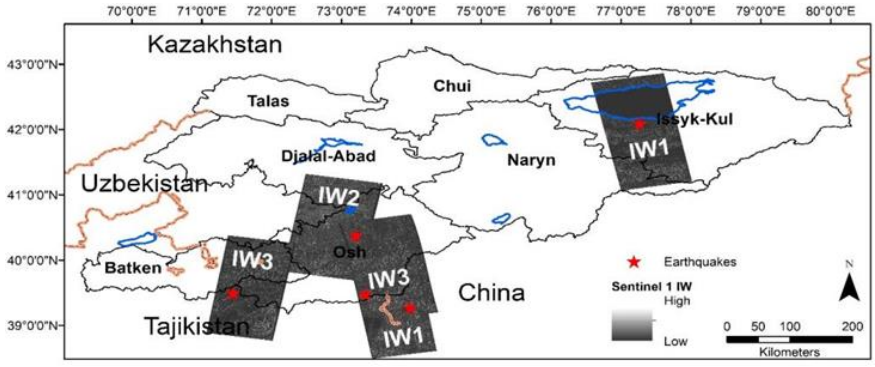

Figure 1: Map of the selected earthquakes and Sentinel-1 IW images

Table 1: Details of earthquake parameters and Sentinel-1 data sets

N	Earthquake Date	Location, Country	Long.; Latit.	Magnitude Depth	Date 1; Date 2	Track number	Temporal; Perpendicular
1	14.11.2014	Kadji-Say, Kyrgyzstan	77.22; 42.12	5.4 Mw 18.6 km	02.11.2014 26.11.2014	056 Ascending	24 days 44.12 m
2	17.11.2015	Taldyk, Kyrgyzstan	73.17; 40.32	5.6 Mw 15.6 km	25.10.2015 18.11.2015	05 Descending	24 days 6 m
3	26.06.2016	Sary-Tash, Kyrgyzstan	73.32; 39.43	6.4 Mw 13.6 km	15.06.2016 09.07.2016	100 Ascending	24 days 13 m
4	25.11.2016	Akto, China	73.95; 39.16	6.6 Mw 17 km	13.11.2016 07.12.2016	027 Ascending	24 days 99 m
5	03.05.2017	Karamyk, Tajikistan	71.43; 39.45	6 Mw 13 km	29.04.2017 11.05.2017	05 Descending	12 days 70 m

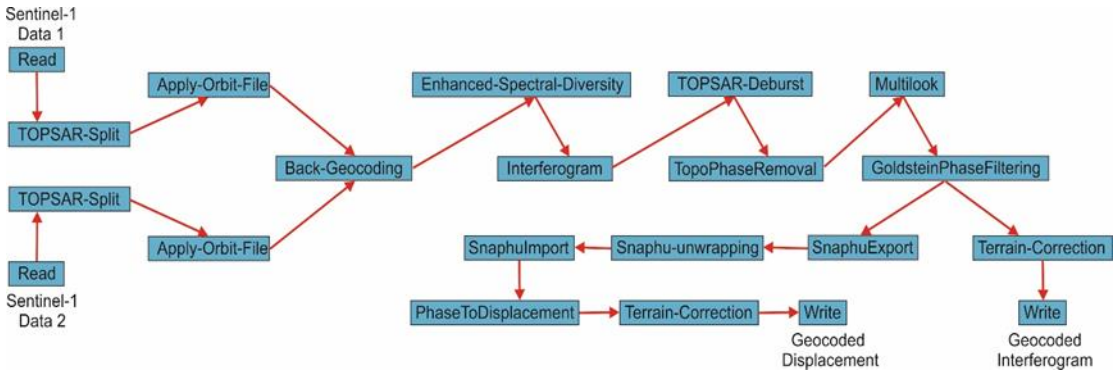

Figure 2: Graph of the steps processed for Sentinel-1 data by using SNAP software

4.2 The Interferometric Processing

The Sentinel-1 data acquired has the Level-1 of the Single Look Complex (SLC) data format. These datasets were processed by using the ESA's Sentinel Application Platform (SNAP) software. We used 8.0.9 software version accessible through the STEP – Scientific Toolbox Exploitation Platform (https://step.esa.int/main/). SNAP is publically accessible software with number of algorithms and possibility to use a Graph Builder tool. This tool allows collecting available operators and connecting nodes to their sources, which can be saved as an XML file. The created graph builder in SNAP software for the Interferometric analysis is illustrated on Figure 2 and the used operators in the processing chain are briefly described below.

The first step is co-registration of two Sentinel-1 Interferometric Wide (IW) images that is fundamental in interferogram generation. Image co-registration is the alignment of two pair images, where the pixels of the slave image correspond to the master image for getting an identical area [13]. The first image acquired before earthquake has been selected as the master image and the second acquired after event as the slave image. Before starting processing analysis, it is important to make a visual analysis of the Sentinel-1 data by using GIS in order to know the sub-swath and bursts covering earthquake epicenter.

The processing starts with the reading of the master and slave images. The next TOPSAR-Split is applied to each data for the selection of the corresponding IW swath, VV type Polarization and some bursts which cover a location of an earthquake event. It is known that man-made features are more clearly shown in the VV Polarization than VH Polarization because it provides higher coherency in an image. The orbits of two split products were downloaded by SNAP software and the extracted Orbit-file provided accurate information about the satellite position during the SAR data acquisition. The burst-by-burst co-registration of both images is achieved by the Back-Geocoding, where precise orbital information from ESA and a Shuttle Radar Topography Mission (SRTM) with 1 arc-second (30m) Digital Elevation Model (DEM) from the National Aeronautics and Space Agency (NASA) had been used. For increasing the precision of the image co-registration, the Enhanced Spectral Diversity (ESD) technique is applied. It exploits the data in the overlap regions of adjacent bursts within a sub-swath. ESD estimates range and azimuth shifts to each burst in overlap region by averaging from all bursts to obtain the final range and azimuth shift for the whole image [23].

The differenced phases of two radar images after precise coregistration formed a new image called an interferogram. It is achieved by multiplying of the first image with the complex conjugate of the second image [16].The computation of the complex interferogram - v_i can be written as [14]:

$$v_i = u_1 u_2^*$$

Equation 1

where: u_1 is the first image, and u_2^* is the complex conjugation of the second images. The interferometric phase in interferogram is represented with one cycle of color or pattern of fringes in terms of 2π radians [16]. The fringe contains the desired information on land elevation and ground deformation [13]. The difference of phase information of two SAR images is called interferometric phase [12] - $\Delta\emptyset$ is proportional to the travel path length difference ΔR divided by the transmitted radar wavelength - λ, [14]:

$$\Delta\emptyset = \emptyset_1 - \emptyset_2 = \frac{4\pi}{\lambda}\Delta R$$

Equation 2

The difference between path length R_1 and R_2 of two radar signals is given as [24]:

$$\Delta R = R_1 - R_2$$

Equation 3

Mostly, the interferometric phase is effected by different factors that contribute to the phase difference in the form as [24]:

$$\Delta\emptyset = \Delta\emptyset_{flat} + \Delta\emptyset_{topo} + \Delta\emptyset_{dis} + \Delta\emptyset_{atm} + \Delta\emptyset_{noi}$$

Equation 4

where: $\Delta\emptyset_{flat}$ is the flat earth phase;
$\Delta\emptyset_{topo}$ is the phase related with topography;
$\Delta\emptyset_{dis}$is the phase affected by surface deformation;
$\Delta\emptyset_{atm}$is the phase of delay caused by atmospheric conditions;
$\Delta\emptyset_{noi}$ is the phase of noise resulting from temporal, geometric and volumetric decorrelation.

Besides the interferometric processing, the coherence is formed as a separate image. It measures a quality for the interferogram and provides valuable information about the land surface types. The interferometric coherence - γ is a magnitude of the complex correlation coefficient between two images, which is expressed as [11]:

$$\gamma = \frac{E[u_1 u_2^*]}{\sqrt{E[|u_1|^2]E[|u_2|^2]}}$$

Equation 5

where: E is the expected statistical value,
u_1 and u_2 the amplitude of two images.

Up to now, each burst has been as separate SLC image processed by containing the black-fill demarcation between the single bursts. To remove it the TOPSAR-Deburst is applied to the Interferogram for merging every burst with its adjacent burst in azimuth direction by preserving the phase information. The topographic phase was subtracted from the processed interferogram by using the SRTM DEM data at 30 m resolution to produce a differential interferogram. Usually, the speckle noise appears to the original SAR images. The reduction of speckle appearance and the improvement of image quality achieved by applying Multilook, which helps to decrease the spatial resolution of the processed data without losing the information in the interferogram [14]. By the use of multilook factors equal to 5 in the range direction and 1 in the azimuth direction, a ground range resolution results in approximately 15 meters. The differential interferogram often impeded by noise from temporal and geometric decorrelation. The phase information in decorrelated regions cannot restore fringes, but the visibility appearances of fringes in the interferogram were significantly improved and the phase noise was reduced by using of a power spectrum filter [25]. It makes smooth of the phase fringes in regions of good coherence that has high correlation, but the amount of noise remains in regions of low correlation.

In the filtered interferogram, the interferometric phase is ambiguous and the phase only known within scale of 2-π radians. In order to recover the corresponding topographic height information, it is necessary to unwrap interferometric phase. The unwrapping solves the ambiguity of phase by adding the integer number of 2-π to the fringes of interferogram. The phase unwrapping process is realized using the SNAPHU Unwrapping plugin in SNAP software.

The most complicated stage in interferometric data processing is the phase unwrapping that consisted on three steps by use the SNAPHU Unwrapping plugin in SNAP software; 1) Export of interferometric data by converting into a format compatible with the SNAPHU; 2) Unwrapping of interferometric phase that referred as the wrapped phase. It is necessary to mention, that the unwrapped phase data does not contain any metadata information. 3) Import of the unwrapped phase by converting back to the SNAP format. The required metadata for the unwrapped phase is added from the wrapped phase such as they have an identical geometry. The unwrapped phase is a continuous raster data with radian units, which need the conversion to a metric measurement.

It is achieved by using the Phase to Displacement operator, where the unwrapped phase values were converted into the ground changes along the Line-of-Sight (LOS) [20]. The LOS is the line between the satellite and a target on the ground. The produced image looks very similar to the unwrapped phase, but the only difference is in the values of pixels representing its displacement in metric values. The positive values represent a mean uplift and the negative values are a mean subsidence on the displacement map.

Finally, the Terrain Correction was applied for the differential interferogram, interferometric coherence and displacement datasets in order to convert from the satellite azimuth-range coordinate into the WGS-84 geographic coordinate system with the consideration of the SRTM DEM data with 30 m resolution.

5. Results and Discussion

5.1 The 2014 Kadji-Sai earthquake, Kyrgyzstan

On November 14, 2014 at 07:25 local time, an earthquake occurred in the South of the Issyk-Kul region in Kyrgyzstan. The earthquake event was identified with a magnitude Mw=5.4 and depth 18.6km by the *United States Geological Survey* (USGS), a magnitude of Mpv=6.2 and a depth of 20km by the Kyrgyz Digital Network (KRNET) belonging to the Institute of Seismology of the Kyrgyz Republic. The earthquake epicenter was located 14 km away from the village of Kadji-Sai. Tremors were felt in the coastal settlements of the Issyk-Kul region, as well as in the capital city of Bishkek, Kyrgyzstan [26].

According to the field observation materials and taking into account the geological conditions of the area of interest, a theoretic isoseismic map was created. Figure 3, shows the epicenter location of earthquake and its intensity distribution covering the settlements in this region. Here, the epicenter is located on the territory of the Ton district, where the villages of Kadji-Say, Kadji-Saz and Korgon-Bulak fall into the zone of ground shaking intensity of I=7 on the MSK-64 scale [6]. The earthquake intensity from I=6 to I=6.5 scales affected several villages of Ton and Djety-Oguz districts of the Issyk-Kul region. In the past, several strong earthquakes have occurred in Ton and Djety-Oguz districts. Most known are Kadji-Say earthquake in 1940 and Barskoon earthquakes occurred in 1965, 1979, 1980 and 1996 years [19]. These earthquake magnitudes were observed to be between 5≤ M< 6. During the Kadji-Say earthquake no human casualties occurred, but many buildings were impacted by different levels of damages in the Issyk-Kul region.

For the analysis of earthquake deformation detectability caused by the Kadji-Say earthquake occurred on November 14, 2014, the Sentinel-1A images captured on November 02, 2014 and November 26, 2104 along the ascending track-056 have been used. These two pairs of images have 24-days temporal baseline and perpendicular baseline of 44 m. The epicenter of the Kadji-Say earthquake covered the Sentinel-1 IW1 sub-swath that was selected for the interferometric processing. In Figure 4(a) coseismic interferogram shows the significant decorrelation, where the Kadji-Sai earthquake was considered as not detected. Here, the surface of Issyk-Kul Lake is masked out such as water basins have no correlation and appears noisy due to constantly moving water waves [16]. The reason of decorrelation without considering a low magnitude earthquake might also be related to the presence of high mountainous relief and the water vapor pressure in the troposphere. Due to the decorrelation, a surface displacement was not generated.

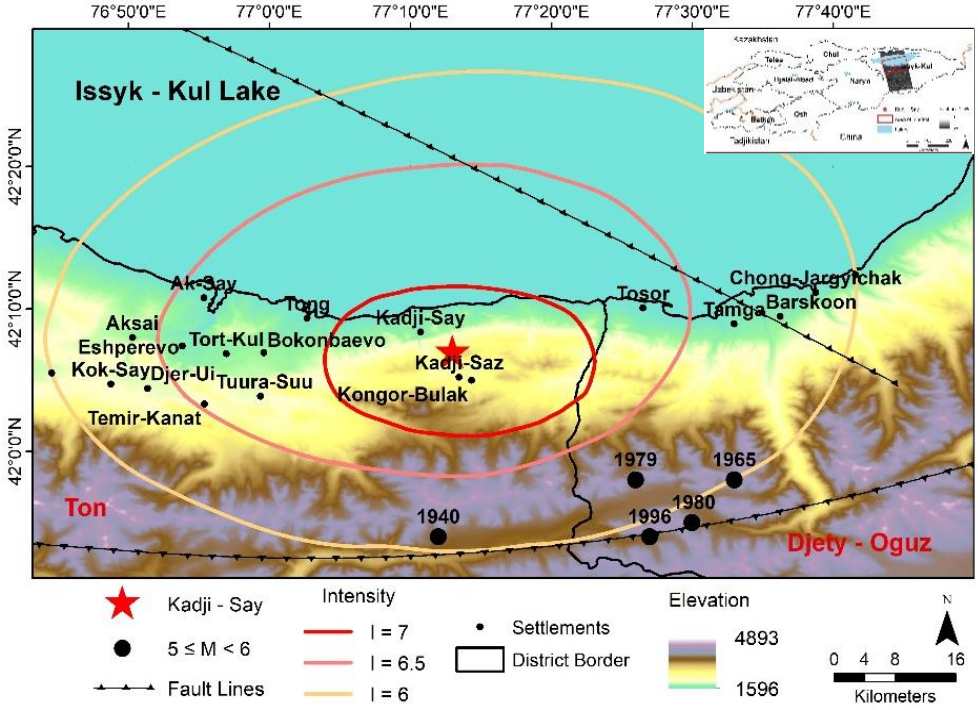

Figure 3: The Kadji-Say earthquake intensity map

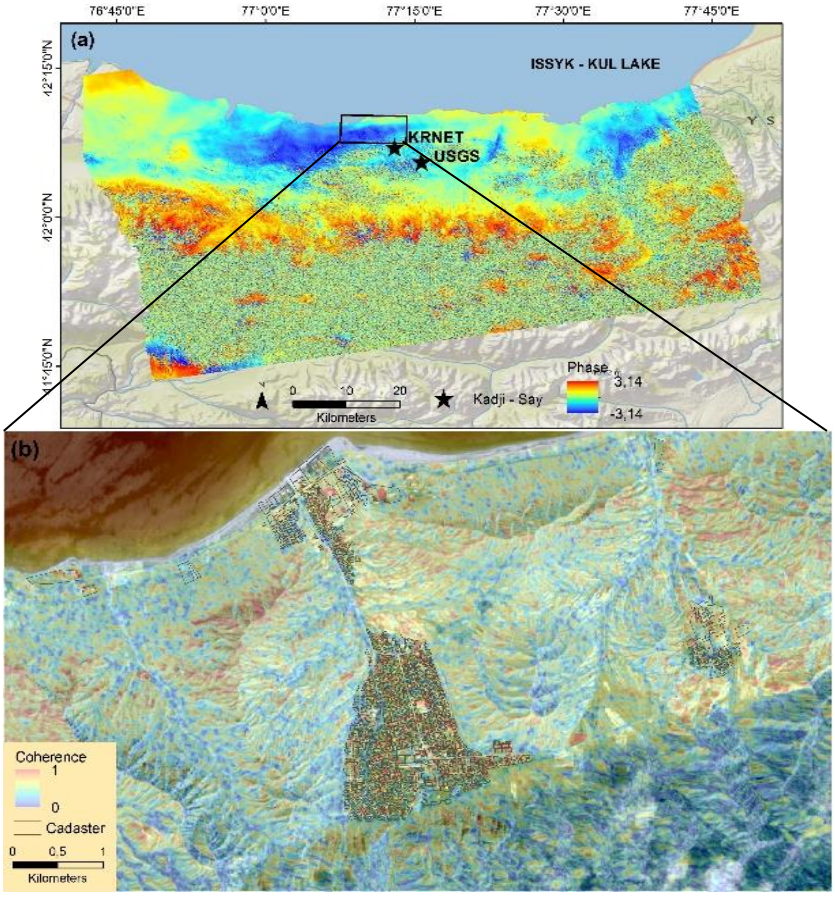

Figure 4: The Kadji-Say earthquake (a) Coseismic Interferogram, (b) Coherence map

In Figure 4(b) shows a coherence map of the village Kadji-Say, which was the mostly affected by an earthquake. In this village, several buildings have obtained a large crack on the walls and at the corner junctions. The cadastral map and the Sentinel-2 image captured on August 09, 2016 have been used as the background image. The coseismic coherence value ranges from 0 to 1. The human-made features and rock areas had a high coherence value.

5.2 The 2015 Taldyk earthquake, Kyrgyzstan

On November 17, 2015 at 17:29 local time an earthquake occurred in the South Fergana zone of the Osh region in Kyrgyzstan. The earthquake event has been detected with a magnitude of Mw=5.6 and depth 15.6 km by the USGS, a magnitude of Mpv=6.4 and depth 13km by the KRNET. This earthquake followed by numerous aftershocks. The epicenter of the main event located near to Taldyk village belonging to Kara-Suu district of the Osh region, Kyrgyzstan [27]. Developed theoretical isoseismic in Figure 5 shows that the settlements of Taldyk, Bek-Jar, Kara-Seget, Laglan, and Langar were felt with ground shaking intensity of I=7 on the MSK-64 scale [6]. In the settlements of Bash-Bulak, Kyzyl-Tuu and Kok-Bel, the earthquake intensity was observed between I=6 and I=7. The strong ground shaking intensity from I=7 to I=5 in the MSK-64 scale were felt in the settlements of Osh region, that is characterized by a high population density [27].

In the past, near to the epicenter of Taldyk earthquake, numerous strong and destructive earthquakes occurred with a magnitude of $5 \leq M < 7$. For instance, there were Nookat earthquake in 1895 (M=5.8; I=6-7), Andijan earthquake in 1902 (M=6.4; I=8-9), Ayim earthquake 1903 (M=6.1; I=8), Kurshab earthquake in 1924 (M=6.5; I=8-9), Naiman earthquake in 1947 (M=5.9, I=8), Kochkor-Ata earthquake in 1992 (M=6.1; I=8), etc. It is necessary to mention, that Kurshab village was destroyed in 1924 and Andijan city in Uzbekistan was destroyed in 1902 [19]. During the Taldyk earthquake, no human casualties occurred, but many buildings experienced different levels of damages in the Osh region.

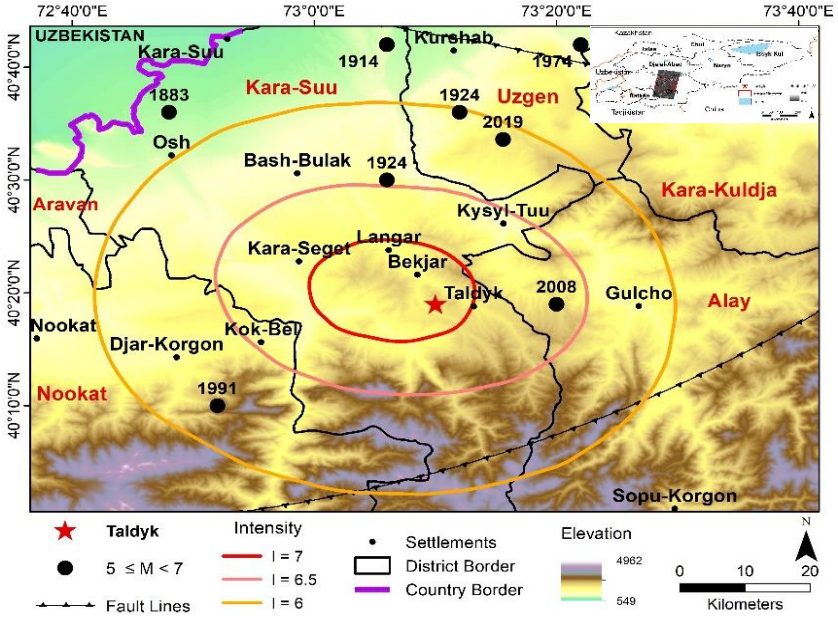

Figure 5: The Taldyk earthquake intensity map

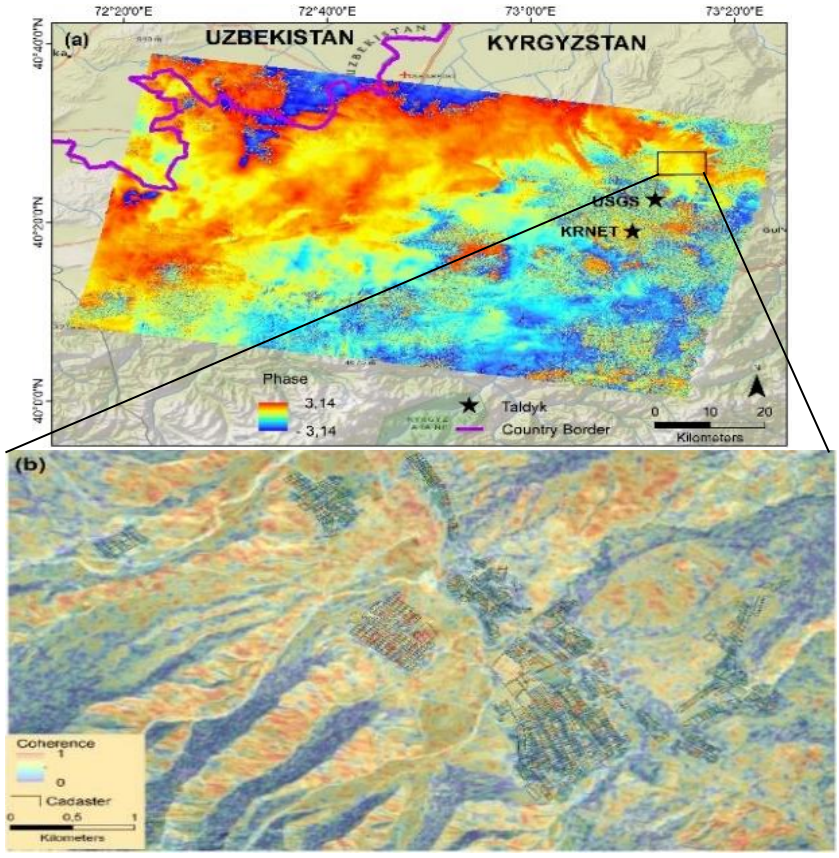

Figure 6: The Taldyk earthquake (a) Coseismic Interferogram, (b) Coherence map

Two Sentinel-1A pairs of images along the descending orbit with track number 05 acquired on October 25, 2015 and November 18, 2015 were used for the ground deformation analysis affected by the Taldyk earthquake occurred on November 17, 2015. The selected satellite images have a time-span of 24 days and perpendicular baseline of 6 m. The coseismic interferogram in Figure 6(a) does not give sufficient details in the area of research interest to identify the Taldyk earthquake. There are displayed partial concentric fringes on the eastern and southern parts of the earthquake epicenter area. It has low changes of the interferometric phases. But it is not clear to identify an earthquake signal. The coseismic interferogram shows the significant decorrelation and the earthquake deformation considered as not detected event. The decorrelation might relate to the availability of high slopes in the mountainous areas. The most affected villages were Bash-Bulak, Kyzyl-Tuu and Kok-Bel. The coherence map for these regions is shown in Figure 6(b). The cadastral data and satellite image of Sentinel-2 acquired on August 2, 2016 was used as the background picture for this region. In these settlement areas, the poorly constructed buildings of adobe types were mostly damaged. Based on the values of the coherence map, the built-up areas were ranging from 0.5 to 0.9. The coherence statistics will be focused for building damage detection analysis in further studies.

5.3 The 2016 Kysyl-Art earthquake, Kyrgyzstan

On June 26, 2016 at 17:17 local time, the Kysyl-Art earthquake occurred in southwest of Kyrgyzstan. This earthquake has been detected with a magnitude of Mw=6.4 and depth 13km by the USGS, a magnitude Mpv=6.5 and depth 10km by the KRNET. The main tremor of this seismic event was accompanied by numerous aftershocks. The epicenter of the Kysyl-Art earthquake is located on the northern slope of the Zaalai Range, 27 kilometers south of Sary-Tash village, 9 km southeast of the Bor-Debe village, and 6 km east of the highway directing to the Kyzyl-Art pass [28].

The produced Isoseismic map in Figure 7 shows that the earthquake intensity of I=7.5 reached to the village of Bor-Dobo. The next villages Sary-Tash, Kok-Bulak and Archa-Bulak were felt an intensity of I=6.6 scale. The ground shaking intensity from I=7.5 to I=6 in MSK-64 scale [6] were reached to the most settlements of the Alai district of the Osh region, which are characterized by low population density [28]. Many people living in high mountainous zone are vulnerable to various natural disasters which occur regularly. In the past, very strong earthquakes occurred here more often than in other seismically active regions of Central Asia. For instance, the Karakul earthquake in 1963 (M=6.6, I=7), the Daroot-Korgon in 1978 (M=6.8, I=7), the Alay in 1983 (M=6.1, I=7-8), the Alay-Nura in 2008 (M=6.7; I=6-7) and other strong earthquakes occurred in this region [19].

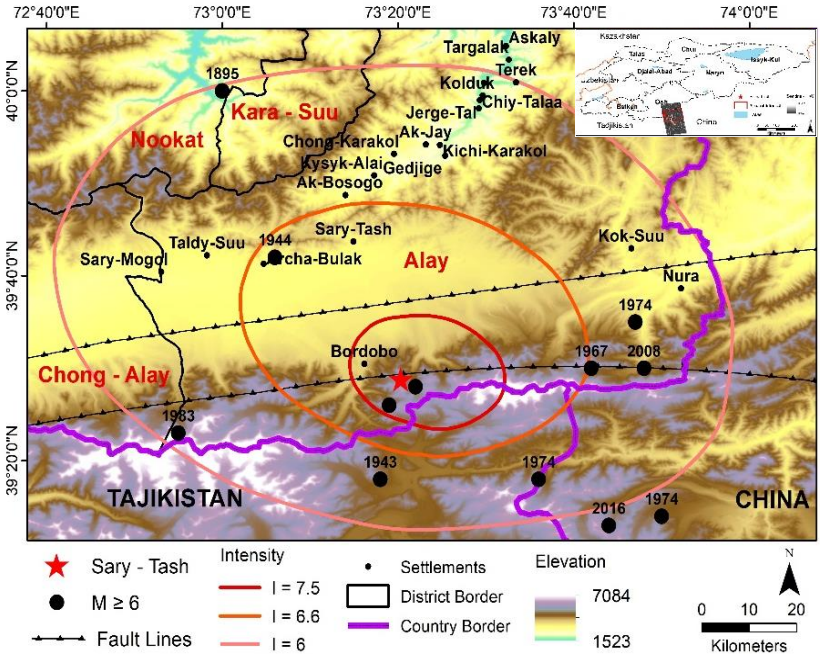

Figure 7: The Kyzyl-Art earthquake intensity map

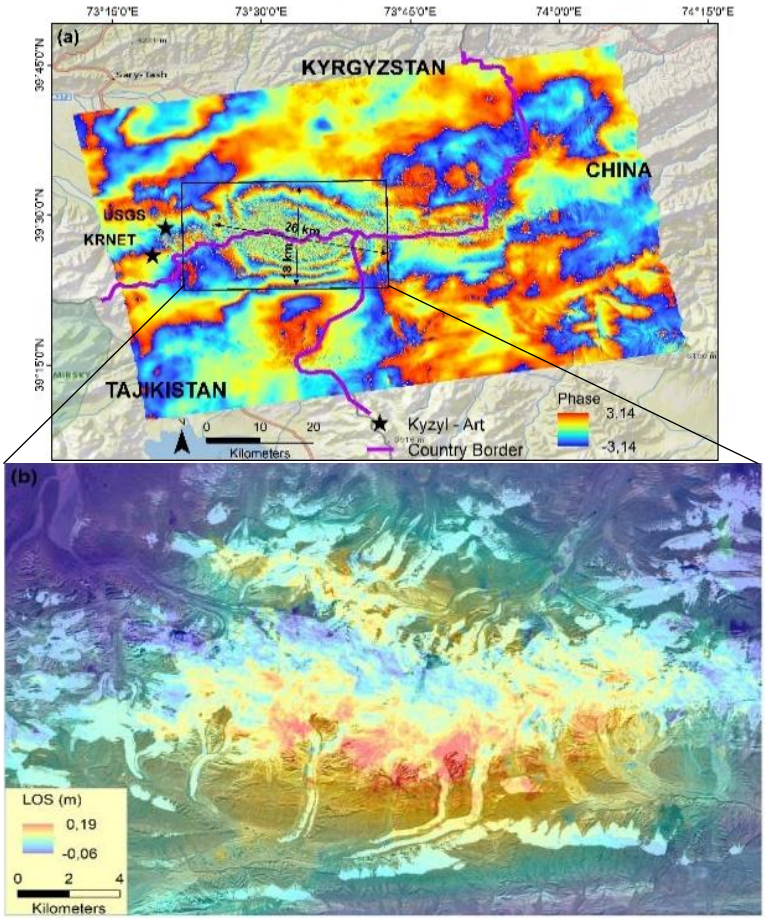

Figure 8: The Kyzyl-Art earthquake (a) Coseismic Interferogram, (b) Displacement map

The Kysyl-Art earthquake did not cause any human injuries but many buildings have received different levels of damages in the Osh region. In addition, this earthquake induced landslide in mountainous areas. Following the Kysyl-Art earthquake on June 26, 2016, the ascending track 100 of the Sentinel-1A images captured on June 15, 2016 and July 09, 2016 for the investigation of the earthquake deformation detection have been processed. Acquired images covered the study area with a temporal baseline of 24 days and perpendicular baseline of 13 m. In Figure 8(a) coseismic interferogram shows two concentric fringes in the left side of image, where the Kyzyl-Art earthquake classified as detected event. The interferometric fringes characterize of ground deformation that extends with about 28 km long and 18 km width in transboundary region between Kyrgyzstan, Tajikistan and China.

The earthquake deformation area is the Zaalai Ridge with high mountains covered in snow and glacier. According to the world topographic map, the elevation ranges from 3500 m to 6616 m above sea level. The cloud free optical satellite image by Sentinel-2 acquired on July 07, 2016 has been used for visual analysis and as the background image for the displacement map in Figure 8(b). This image shows the parts of dislocations such as landslides induced by the Kyzyl-Art earthquake. It displays the ground displacement in LOS that indicates uplift up to 19 cm and subsidence of 6 cm. The uplift might indicate of the glacier and landslide movements.

5.4 The 2016 Aketao Earthquake, China

On November 25, 2016 at 20:24 local time, an earthquake occurred near the southern border of Kyrgyzstan. The earthquake magnitude of Mw=6.6 and depth of 19.1 km by USGS, a magnitude of Mpv= 6.8 and depth of 14.1 km were estimated by KRNET. Its epicenter was located on the territory of neighboring China, in the Aketao County of the Kizilsuu-Kirghiz Autonomous Prefecture of the Xinjiang Uygur Autonomous Region, China. The numerous strong aftershocks were sensible in many settlements of Kyrgyzstan and neighboring countries [29].

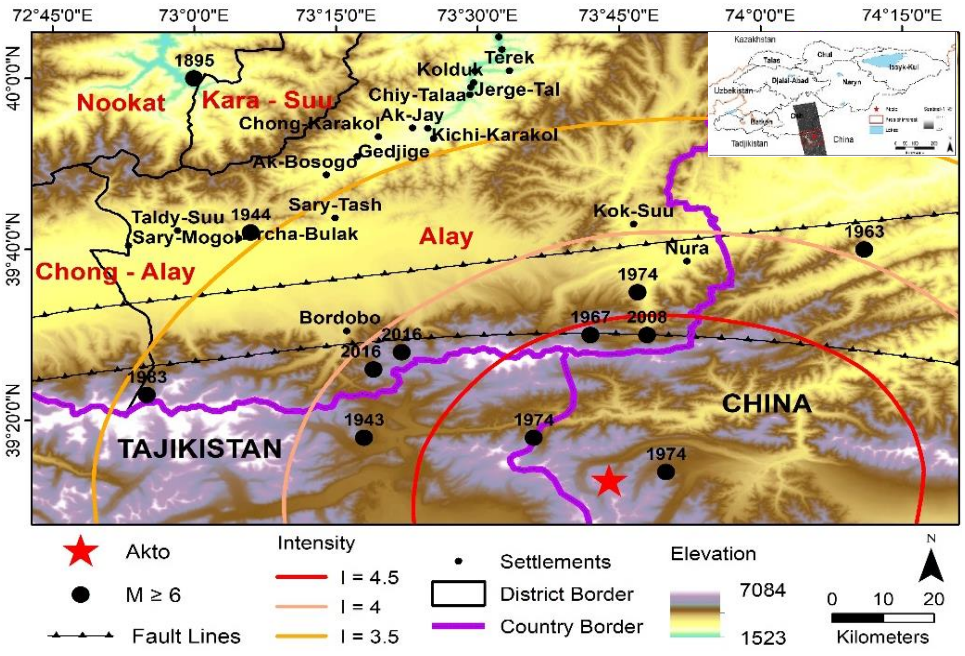

Figure 9: The Aketao earthquake intensity map

Aketao earthquake occurred in a sparsely populated area and therefore a large number of victims and destructions have not observed. This earthquake caused panic among the people on the border villages of Kyrgyzstan [29]. Figure 9 shows a theoretical isoseismic map of this earthquake. The earthquake manifested with an intensity of I=4.5 in MSK-64 scale [6] in the territory of Osh region, Kyrgyzstan. Historically, number of strong earthquakes occurred in this area. As an example, the strongest earthquake event was the Markansuiskoe in 1974 (M=7.3. I=7-8) which occurred in China, 30 km from the southern border of Kyrgyzstan. Both Aketao and Markansuiskoe earthquakes were preceded by a foreshock and have been accompanied by a large the number of aftershocks. The next Alay-Nura earthquake in 2008 (M=6.7; I=6-7) completely destroyed the village of Nura in the eastern part of the Alai Valley in Kyrgyzstan and 74 people died [19]. Aketao earthquake region is characterized as high level of seismically hazardous that affects not only for the territory of China, but also to the south of Kyrgyzstan [29].

Sentinel-1A images acquired on November 13, 2016 and December 3, 2016 along the ascending track-027 for the Aketao earthquake occurred on November 25, 2016 were used for this research. Applied two satellite images have a temporal line of 24 days and perpendicular baseline of 102 m. In Figure 10(a) coseismic interferogram has sufficiently high correlation between two images, where the Aketao earthquake can be identified as deformation detected event. The interferometric fringes are formed on two places on the image. The first deformation on the west part nearby the earthquake epicenter has a wide extension with about 27 km long and 21 km in width. It clearly shows three concentric fringes. The second deformation on the eastern part has short-dense extension surrounding in about 16 km length and represents four concentric fringes. Since the Sentinel-1 Interferometric data is used, concentric fringe color characterizes 2.8 cm change. The earthquake deformation area is the Pamir Mountain which lies at the collision between the Indian and the Eurasian plates. The Sentinel-2 acquired on July 20, 2016 has been used for visual analysis of the displacement map in Figure 10(b). It displays of the surface displacement with the maximum uplift of 15 cm and the subsidence of 13 cm. The surface uplift might indicate the land movements from the mountains, while the subsidence of soils nearby the hydrological areas.

5.5 The 2017 Karamyk Earthquake, Tajikistan

On May 3, 2017 at 09:47 local time, an earthquake occurred at the border of Tajikistan and Kyrgyzstan. The earthquake with magnitude of Mw=6 and depth of 11 km by the USGS, a magnitude of Mpv= 6.5 and depth of 13 km were estimated by the KRNET. The earthquake followed by numerous aftershocks. The epicenter of event was located at the Lakhsh district, the formerly known as Jerge-Tal region.

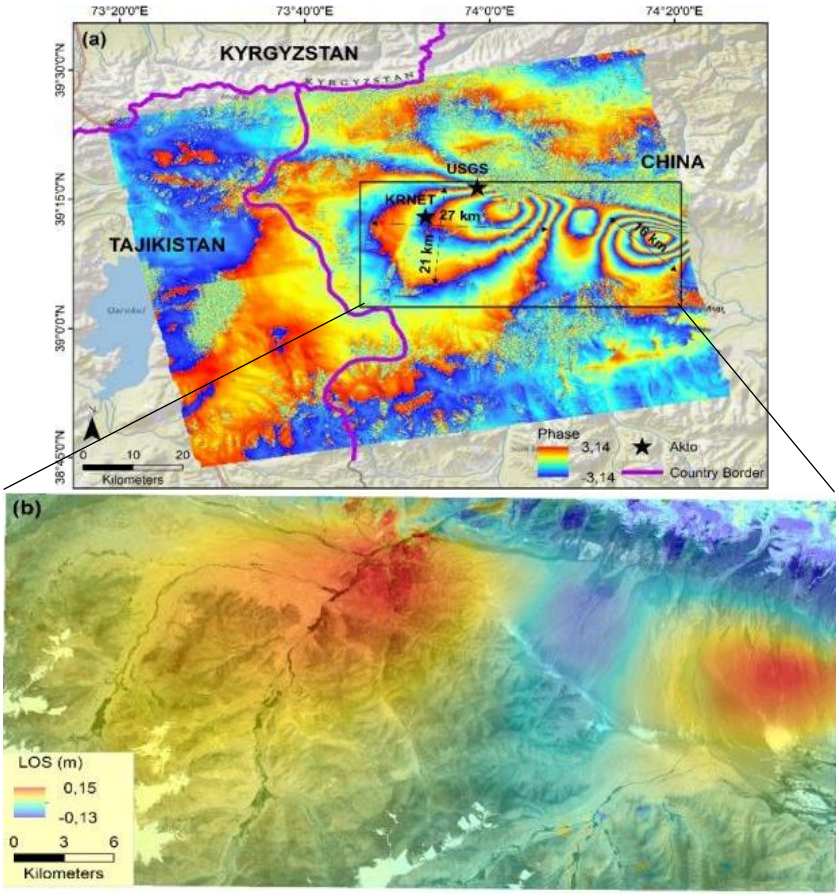

Figure 10: The Aketao earthquake (a) Coseismic Interferogram, (b) Displacement map

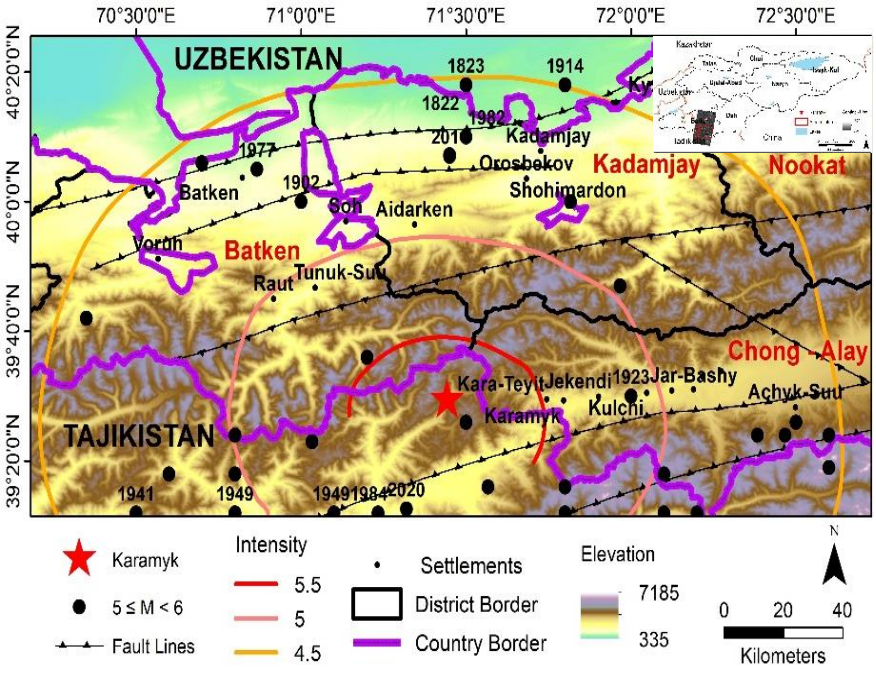

Figure 11: The Karamyk earthquake intensity map

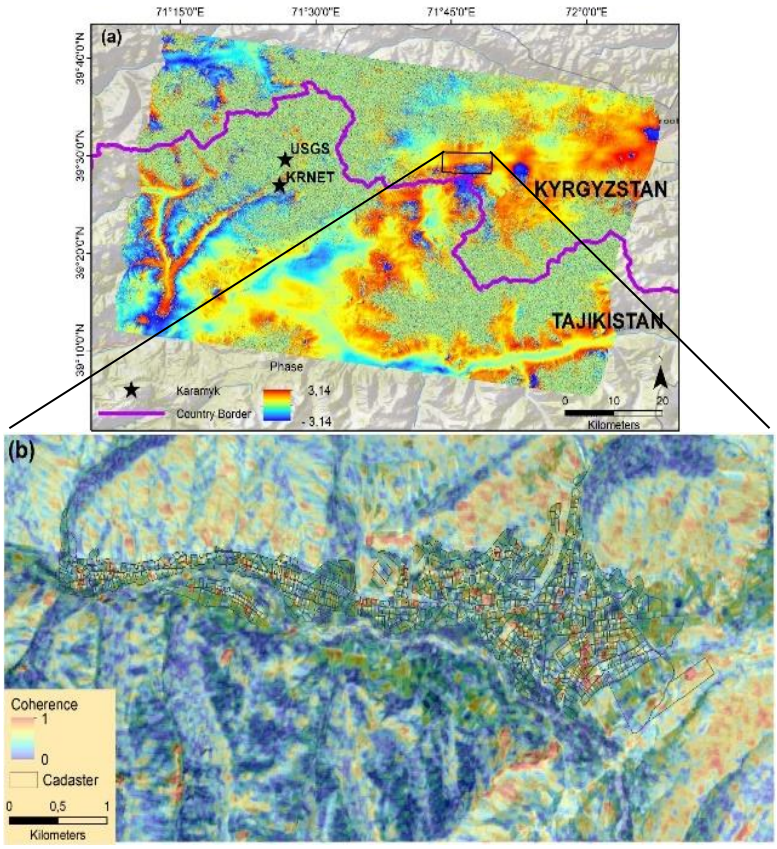

Figure 12: The Karamyk earthquake (a) Coseismic Interferogram, (b) Coherence map

The earthquake intensity reached I=6 in the MSK-64 scale [6], where several villages in the territory of Tajikistan were severely affected [30]. The ground shaking covered an extensive territory of Kyrgyzstan. Nearby the earthquake with epicenter about 30 km was located the Karamyk village, which belongs to the Chon-Alai district of the Osh region in Kyrgyzstan. Figure 11 characterizes a theoretical isoseismic map of the Karamyk earthquake. In the region of the villages Karamyk, Kara-Teyit, Shibee and Jekendy, earthquake was observed with the intensity of I=6 in the MSK-64 scale [6]. The earthquake with intensity of I=6 were observed in the most settlements of the Chong-Alay district and intensity I=5 in MSK-64 scale reached the Kadamjay and Batken districts in Kyrgyzstan [28].

In the past, the most historically strong earthquakes epicenters were located in the Southern-Fergana tectonic plate. For example, the Garmskoe earthquake in 1941 (M=6.4, I=9), the Khaitskoe in 1949 (M=7.4, I=9-10), the Isfara-Batken in 1977 (M=6.3, I=7-8), the Kanskoe in 2011 (M=6.2, I=8-9) and other strong earthquakes occurred in this region [19]. The Karamyk earthquake did not cause any human injuries, but many residential and public buildings had different level of damages.

The descending track 05 of the Sentinel-1A image pairs acquired on April 29, 2017 and May 11, 2017 have been applied for the Karamyk earthquake occurred on May 3, 2017. The acquired images covering the study area have a temporal baseline of 12 days and perpendicular baseline of 70 m. According to eyewitnesses, this earthquake induced a rupture with a length of more than 100 m on the mountain lakeside of the territory of Tajikistan [30]. The coseismic interferogram in Figure 12(a) shows low correlation to identify an earthquake deformation. It has a several noise in the interferogram. There are containing very small regions with interferometric phase changes in the surrounding of the earthquake epicenter area. But it is not sufficient to identify an earthquake deformation signal. Decorrelation might relate to the vegetation fast growth in spring season, which makes problematic to identify an earthquake signal. Figure 12(b) represents a coherence map over the village Karamyk in Kyrgyzstan. The Sentinel-2 image captured on August 22, 2017 was used as the background image.

In this village, the poorly constructed residential and public buildings were mostly damaged. According to the coherence map, the vegetation and water have low coherence, while the built-up areas have high values ranging from 0.5 to 0.9. In the future, the coherence change study will be applied for building damage detection analysis.

6. Conclusions

Historically, the Kyrgyz Republic and neighboring countries have experienced numerous strong earthquakes which caused huge economic and human losses, damage of buildings and engineering-structures. For our research task, we selected 5 earthquake events for 2014-2017 years, where 3 earthquake epicenters were located in the territory of the Kyrgyz Republic and 2 earthquakes in the neighboring countries of China and Tajikistan. The selection criteria of an earthquake based on magnitude Mw>5 and hypocentral depth below h<20 km. According to the field observations it was possible to develop theoretic isoseismic maps. These maps provided valuable information regarding the spatial distribution of ground shaking intensity of earthquakes. The intensity information covering the settlement area for generating of rapid information about the buildings and population exposure statistics plays an important role for earthquake vulnerability and seismic risk assessment studies. We applied a Differential Inteferometric Synthetic Aperture Radar (DInSAR) technique to the Sentinel-1 Interferometric data acquired before and after an earthquake event. The pairs of Sentinel-1 images were processed using the Sentinel Application Platform (SNAP) software that is publicly accessible software. The developed processing chain of graph builder in the SNAP software has been applied for each event to produce a surface deformation and displacement maps.

As the result, a coseismic interferogram and coherence map have been produced by the cross-multiplication between the master and the slave images. The amplitude of both images was multiplied while the interferometric phase shows differences in phase of two images. The interferometric phase were converted to a metric values that measures of ground changes along the Line-of-Sight (LOS). Based on our study results we can conclude that a detection of earthquake deformation is strongly dependent on earthquake magnitude and hypocenter depth. This was reflected in the fact that not all the selected earthquakes produced concentric fringes in the coseismic interferograms. In our study, where the2016 Kysyl-Art and the 2016 Aketao earthquakes have a greater magnitude of Mw>6. The produced coseismic interferograms successfully provided a clear visualization in the form of colour fringes, which presented earthquake deformations. The displacement induced by these earthquakes represented ground changes indicating from uplift to subsidence in metric units. Since the Sentinel-1 Interferometric data was used, each concentric fringe color characterizes 2.8 cm of change. The other three earthquakes, the 2014 Kadji-Say, the 2015 Taldyk and the 2017 Karamyk earthquakes have magnitude between Mw>5.0 and Mw≤6.0 with a depth of h>10km. The produced coseismic interferograms of these earthquakes shows the significant decorrelation, where a ground deformation was not detected. Because deeper earthquake will generate less ground deformation. In some research studies, where it was successfully produced a coseismic interferogram for the earthquakes with a magnitude Mw>5 occurred at shallow depth of h<10km.

The decorrelation of used SAR images effect on high slopes of the mountain areas in Kyrgyzstan and change of vegetation response, which makes problematic to clearly identify an earthquake deformation. The 2014 Kadji-Say, the 2015 Taldyk and the 2017 Karamyk earthquakes caused damages of residential and public buildings in rural areas. The affected damage is mainly due to the low seismic resistance of buildings made from local construction materials. Further research will focus on building damage detection using the Coherence Change Detection (CCD) techniques and recovery monitoring using an optical remote sensing data.

References

[1] Kusky, T., (2008). *Earthquakes: Plate Tectonics and Earthquake Hazards*. Infobase Publishing, 1-169.

[2] Udias, A., (1999). *Principles of Seismology*. Cambridge University Press, 1-490.

[3] Richter, C., (1935). An Instrumental Earthquake Magnitude Scale. *Bulletin of the Seismological Society of America*, Vol. 25(1), 1–32.

[4] Sucuoğlu, H. and Akkar, S., (2014). *Basic Earthquake Engineering: From Seismology to Analysis and Design*. Springer International Publishing, 1-288.

[5] Wood, H. and Neumann, F., (1931). Modified Mercalli Intensity Scale of 1931. *Bulletin of the Seismological Society of America*, Vol. 21(4), 277–283.

[6] Medvedev, S., Sponheuer, W. And Karník, V., (1964). Neue Seismische Skala Intensity Scale of Earthquakes, 7. Tagung der Europäischen Seismologischen Kommission vom 24.9. bis 30.9.1962 in Jena, DDR, Berlin: Akademie-Verlag, 69-76.

[7] Grünthal, G., (1998). European Macroseismic Scale 1998 (EMS-98) European Seismological Commission, Sub Commission on Engineering Seismology, Working Group Macroseismic Scales. Conseil de l'Europe, Cahiers du Centre Européen de Géodynamique et de Séismologie, Vol. 15, 1-99.

[8] Bayramov, E., Buchroithner, M. And Kada, M., (2020). Radar Remote Sensing to Supplement Pipeline Surveillance Programs through Measurements of Surface Deformations and Identification of Geohazard Risks. *Remote Sensing*, Vol. 12(23). https://doi.org/10.3390/rs 12233934.

[9] Tronin, A., (2009). Satellite Remote Sensing in Seismology: A Review. *Remote Sensing* Vol. 2,124-150. doi:10.3390/rs2010124

[10] Funning, G. J. and Garcia, A., (2019). A Systematic Study of Earthquake Detectability Using Sentinel-1 Interferometric Wide-Swath Data. *Geophysical Journal International*, Vol. 216(1), 332-349. https://doi.org/10.1093/gji/ggy 426

[11] Bamler, R. and Hartl, P., (1998). Synthetic Aperture Radar Interferometry. *Inverse Problems*, Vol. 14(4), R1–R54.

[12] Rott, H., (2009). Advances in Interferometric Synthetic Aperture Radar (InSAR) in Earth System Science. *Progress in Physical Geography: Earth and Environment*, Vol. 33(6), 769–791. https://doi.org/10.1177/030913330935 0263

[13] Massonnet, D. and Feigl, K. L., (1998). Radar Interferometry and its Application to Changes in the Earth's Surface. *Reviews of Geophysics*, Vol. 36(4), 441-500.

[14] Ferretti, A., (2007). *InSAR Principles: Guidelines for SAR Interferometry Processing and Interpretation.* TM-19. The Netherlands, ESA Publications. https://www.esa.int/esapub/ tm/tm19/TM-19_ptA.pdf

[15] Lillesand, T., Kiefer, R. and Chipman, J., (2015). *Remote Sensing and Image Interpretation.* Seventh Edition. Wiley, 1-736.

[16] Rosen, P., Hensley, S., Joughin, I. R., Li, F. K., Madsen, S., Rodriguez, G. and Goldstein, R. M., (2000). Synthetic Aperture Radar Interferometry. Proceedings of the IEEE, Vol. 88(3), 333-382. https://doi.org/10.1109/5.83 8084.

[17] Massonnet, D., Rossi, M., Carmona, C., Adragna, F., Peltzer, G., Feigl, K. and Rabaute, T., (1993). The Displacement Field of the Landers Earthquake Mapped by Radar Interferometry. *Nature*, Vol. 364, 138-142.

[18] Teshebaeva, K., Sudhaus, H., Echtler, H., Schurr, B. and Roessner, S., (2014). Strain Partitioning at the Eastern Pamir-Alai Revealed through SAR Data Analysis of the 2008 Nura Earthquake. *Geophysical Journal International*. Vol. 198(2), 760–774. https://doi.org/10.1093/ gji/ggu158

[19] Kalmetyeva, Z. A., Mikolaichuk, A. V., Moldobekov, B., Meleshko, A. V., Jantaev, M. M., Zubovich, A. V. and Havenith, H. B., (2009). *Atlas of earthquakes in Kyrgyzstan*. Central-Asian Institute for Applied Geosciences and United Nations International Strategy for Disaster Reduction Secretariat Office in Central Asia, Bishkek. 1-232.

[20] Monterroso, F., Bonano, M., De Luca, C., De Novellis, V., Lanari, R., Manunta, M., Manzo, M., Onorato, G., Valerio, E., Zinno, I. and Casu, F., (2018). Automatic Generation of Co-Seismic Displacement Maps by Using Sentinel-1 Interferometric SAR Data. *Procedia Computer Science*, Vol. 138, 332–337. https://doi.org/10. 1016/j.procs2018.10.047

[21] Jasim, A. and Hassan, M., (2020). Sentinel-1 Processing and Analysis to Estimate Ground Displacement and Identify Activation Faults, Case Study of the 2017 Mw 7.3 Earthquake, Near the Iraq-Iran Border. *Iraqi Geological Journal*. Vol. 53(1), 93-113.

[22] Torres, R., Snoeij, P., Geudtner, D., Bibby, D., Davidson, M., Evert Attema, E., Potin, P., Rommen, B., Floury, N., Mike Brown, M., Traver, I. N., Deghaye, P., Duesmann, B., Rosich, B., Miranda, N., Bruno, C., L'Abbate, M., Croci, R., Pietropaolo, A., Huchler, M. and Rostan, F., (2012). GMES Sentinel-1 Mission. *Remote Sensing of Environment.* Vol. 120, 9–24. https://doi.org/10.1016/j.rse.2011.05.028

[23] Martinez, N. Y., Iraola, P. P., Gonzalez, F. R., Brcic, R., Shau, R., Geudtner, D., Eineder, M. and Bamler, R., (2016). Interferometric Processing of Sentinel-1 TOPS Data. *IEEE Transactions on Geoscience and Remote Sensing*. Vol. 54(4), 1-15. https://doi.org/10.1109/TGRS.2015.2497902

[24] Richards, J. A., (2009). *Remote Sesning with Imaging Radar*. Springer-Verlag Berlin Heidelberg, 1-361.

[25] Goldstein, R. and Werner, C., (1998). Radar Interferogram Filtering for Geophysical Applications. Geophysical Research Letters. Vol. 25(21), 4035-4038.

[26] Grebennikova, V.V., Frolova, A.G., Bagmanova, N.Kh., Berezina, A.V., Pershina, E.V., Moldobekova, S. (2020). *Kaji-Sai eartнquake on November 14, 2014 wit Kp =13.7, Mw=5.4, Io=7 (Kyrgyzstan, Southern Issyk-Kul).* Zemletriaseniia Severnoi Evrazii [Earthquakes in Northern Eurasia], 23, 364–374. (In Russ.).

[27] Frolova, A., Grebennikova, V., Bagmanova, N., Berezina, A., Pershina, E. and Moldobekova, S., (2021). Taldyk Earthquake on November 17, 2015 with KR=14.1, Mw=5.5 Kyrgyzstan. *Geophysical Survey of the Russian Academy of Sciences - GS RAS*, 340–348. (In Russ.). https://doi.org/10.35540/1818-6254.2021.24.32

[28] Grebennikova, V.V. and Fortuna, A. B., (2018). Seismicity of the Zaalay Ridge (Pamir-Alay Zone). *Bulletin of the Institute of Seismology of the NAS of the Kyrgyz Republic*. Vol. 1(11), 18-31. (In Russ.).

[29] Abdrahmatov, K.E., Frolova, A.G., Bagmanova, N.Kh., Berezina, A.V., Pershina, E.V., Moldobekova, S. (2020). Aketaosk Earthquake of November 25, 2016 (China) with Kr = 15.4 and its effect on the Territory of Southern Kyrgyzstan. *Bulletin of the Institute of Seismology of the NAS of the Kyrgyz Republic*. Vol. 2(16), 13-22 (In Russ.).

[30] Djuraev, R. U. and Grebennikova, V. V., (2018). Macroseismic Consequences of the Earthquake of 3-6 May, 2017 in the Border Areas of Tajikistan and Kyrgyzstan. *Bulletin of the Institute of Seismology of the NAS of the Kyrgyz Republic*.Vol. 2(12), 25-37 (In Russ.).